We are IntechOpen, the world's leading publisher of Open Access books Built by scientists, for scientists

4,800
Open access books available

122,000
International authors and editors

135M
Downloads

Our authors are among the

154
Countries delivered to

TOP 1%
most cited scientists

12.2%
Contributors from top 500 universities

CLARIVATE ANALYTICS BOOK CITATION INDEX INDEXED

WEB OF SCIENCE™

Selection of our books indexed in the Book Citation Index in Web of Science™ Core Collection (BKCI)

Interested in publishing with us?
Contact book.department@intechopen.com

Numbers displayed above are based on latest data collected.
For more information visit www.intechopen.com

9

Room Temperature Integrated Terahertz Emitters based on Three-Wave Mixing in Semiconductor Microcylinders

A. Taormina[1], A. Andronico[2], F. Ghiglieno[1], S. Ducci[1], I. Favero[1] and G. Leo[1]
[1]*Université Paris Diderot, Laboratoire MPQ – CNRS-UMR 7162,*
[2]*Institute for Genomics and Bioinformatics, University of California Irvine, CA 92697*
[1]*France*
[2]*USA*

1. Introduction

In the last years, the Terahertz (THz) domain has attracted an increasing interest in the scientific community due to the large number of applications that have been identified (Tanouchi, 2007).
Even if many different Terahertz sources - like photomixers, quantum cascade lasers, and photoconductive antennas (Mittleman, 2003) - have been investigated in the past, the fabrication of a compact device operating at room temperature and with an output power at least in the μW range still constitutes a challenge.
A very promising approach to this problem relies on the nonlinear optical process called Difference Frequency Generation (DFG) in materials like III-V semiconductors (Boyd, 2003).
In this chapter, we will propose an efficient, compact, and room-temperature THz emitter based on DFG in semiconductor microcylinders. These are whispering gallery mode (WGM) resonators capable to provide both strong spatial confinement and ultra-high quality factors. Nonlinear optics applications benefit from an ultra-high-Q cavity, since the fields involved in the nonlinear mixing interact for a long time, giving rise to an efficient conversion.
The structure we investigate is based on the technology of GaAs, owing to its wide transparency range (between about 0.9 and 17 μm), large refractive index for strong field confinement, and a huge nonlinear coefficient. Moreover, it offers attracting possibilities in terms of optoelectronic integration and electrical pumping.
After an introductory part about whispering gallery modes, we will present the study of the DFG inside GaAs microcylinders. The evanescent coupling with an external waveguide allows a selective excitation of the pump cavity modes.
At the end, on the theoretical premises of the first part, we will show that an appealingly simple structure can be used to confine both infrared and THz modes. Moreover, embedding self-assembled quantum dots in the cavity allows the integration of the pump sources into the device. With an appropriate choice of the cylinder radius, it is possible to phase match two WGMs with a THz mode, and have a compact, room-temperature THz emitter suitable for electrical pumping.

Source: Recent Optical and Photonic Technologies, Book edited by: Ki Young Kim,
ISBN 978-953-7619-71-8, pp. 450, January 2010, INTECH, Croatia, downloaded from SCIYO.COM

2. Whispering gallery modes

2.1 Microcylinder cavity modes

Whispering gallery modes are the optical modes of microcylinders, and, being the eigenmodes of a 3D structure, they cannot in general be derived analytically. However, the simple approximation we describe in the following (Heebner et al., 2007) can be used to reduce the 3D problem to a more manageable (2+1)D problem[1].

From Maxwell's equations in Fourier space and without source terms, we can easily obtain the familiar wave equation:

$$\nabla^2\vec{F}+\frac{n^2\omega^2}{c^2}\vec{F}=0 \tag{1}$$

where $\vec{F}$ is either $\vec{E}$ or $\vec{H}$, and n is the refractive index (in general frequency dependent) of the medium.

Using the cylindrical coordinates (ρ, θ, x) shown in Fig. 1, equation (1) can be rewritten as:

$$\left(\frac{\partial^2}{\partial\rho^2}+\frac{1}{\rho}\frac{\partial}{\partial\rho}+\frac{1}{\rho^2}\frac{\partial^2}{\partial\rho^2}+\frac{\partial^2}{\partial x^2}+\frac{n^2\omega^2}{c^2}\right)\vec{F}=0 \tag{2}$$

Let us assume that it is possible to classify the modes as purely TE or TM: in the first case, the non-vanishing components are H_x, E_ρ and E_θ, whereas, in the second, they are E_x, H_ρ and H_θ. This assumption, which echoes the optical slab waveguide case, is only approximate but greatly reduces the complexity of the problem: as we will see in the following, it is equivalent to decoupling the in-plane problem from the vertical problem, using the effective index method to take the latter into account (Tamir, 1990).

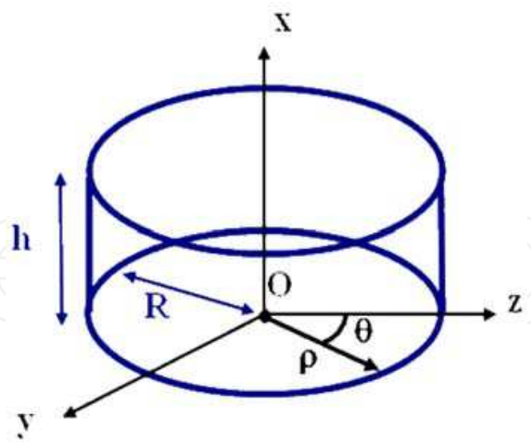

Fig. 1. General scheme of a microcylinder with radius R and thickness h. The cylindrical reference system used in the chapter is also shown.

Returning to Eq. (2) and writing the only independent field component F_x in the factorized form $F_x = \psi(\rho)\,\Theta(\theta)\,G(x)$, we find the following three equations:

[1] Recently, fully vectorial 3D approaches have also been proposed (Armaroli et al., 2008).

$$\begin{cases} \dfrac{d^2G}{dx^2}+\dfrac{\omega^2}{c^2}\left(n^2-n_\xi^2\right)G=0 \\ \dfrac{d^2\Theta}{d\theta^2}+m^2\Theta=0 \\ \dfrac{d^2\Psi}{d\rho^2}+\dfrac{1}{\rho}\dfrac{d\Psi}{d\rho}+\left(\dfrac{n_\xi^2\omega^2}{c^2}-\dfrac{m^2}{\rho^2}\right)\Psi=0 \end{cases} \tag{3}$$

The first equation tells us that G(x) is the eigenfunction of a slab waveguide with effective index n_ξ (ξ = TE/TM), whereas the second can be integrated to obtain $\Theta(\theta) = e^{-im\theta}$, m being the (integer) azimuthal number.
The radial mode dependence is obtained using the last equation in (3): if the microdisk radius is R, then $\psi(\rho)$ can be written in terms of first-kind Bessel functions (for $\rho \le R$) and second-kind Hankel functions (for $\rho > R$):

$$\Psi(\rho)=\begin{cases} NJ_m\left(kn_\xi\rho\right) & \rho\le R \\ NBH_m^{(2)}(k\rho) & \rho>R \end{cases} \tag{4}$$

where N is a normalization constant, $k=\omega/c$, $B=J_m\left(kn_\xi R\right)/H_m^{(2)}(kR)$, and we assume that the microcylinder is surrounded by air.
If we impose the continuity of tangential components $\vec{E}$ and $\vec{H}$, we find the following dispersion relations:

$$\begin{aligned} &\text{TM modes} && n_\xi\frac{\dot{J}_m\left(kn_\xi R\right)}{J_m\left(kn_\xi R\right)}-\frac{\dot{H}_m^{(2)}(kR)}{H_m^{(2)}(kR)}=0 \\ &\text{TE modes} && \frac{\dot{J}_m\left(kn_\xi R\right)}{J_m\left(kn_\xi R\right)}-n_\xi\frac{\dot{H}_m^{(2)}(kR)}{H_m^{(2)}(kR)}=0 \end{aligned} \tag{5}$$

Once these equations are numerically solved with respect to the variable k, we obtain the resonance eigenfrequencies $\tilde{\omega}$ of the cavity.
At this point it is worth stressing that, despite the formal analogy with the optical slab waveguide, the frequency of a WGM is a complex number, even if the effective index n_ξ that appears in equation (3) is real. This is due to the fact that the microcylinder walls are curved and then all its resonances are affected by radiation losses, which can be quantified by defining the WGM quality factor of a resonator mode:

$$Q^{WGM}=\frac{\mathrm{Re}(\tilde{\omega})}{2\mathrm{Im}(\tilde{\omega})} \tag{6}$$

Simply stated, the bent geometry of the microdisk gives rise to a continuous decay rate of the energy confined within the cavity, broadening the resonances linewidth.
Fig. 2 shows the square modulus of equations (5) versus the angular frequency for a microcylinder of radius R = 1 μm and effective index n = 2.2: it is evident that once we establish the structure under investigation (i.e. the disk radius and thickness, and

subsequently the effective index n_ξ) and the azimuthal number m, multiple radial solutions exist. We can then label them by employing an additional integer number p, which is the radial order of the mode and corresponds to the number of field maxima along the radial axis of the microcylinder.

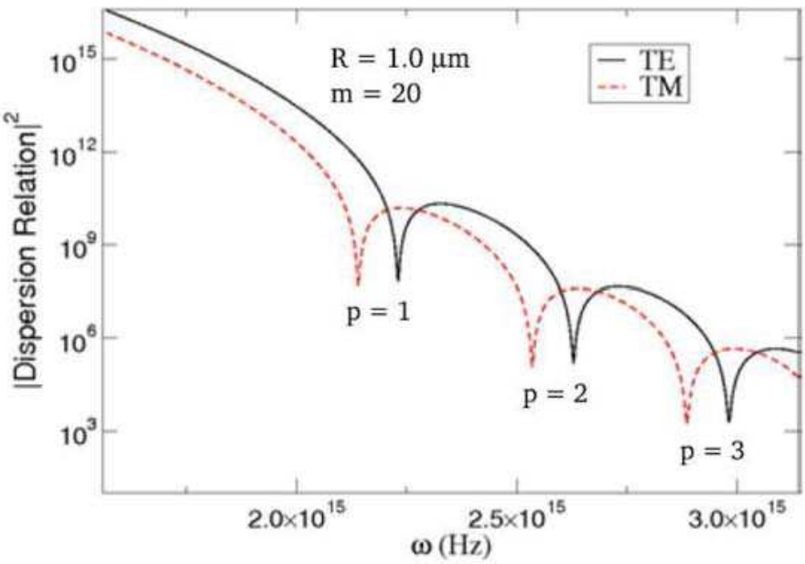

Fig. 2. Square modulus of the dispersion relations (5) versus angular frequency. The azimuthal symmetry of the modes is fixed (m=20): different function dips correspond to different radial order modes, as indicated.

It is interesting to note that higher p order modes have higher frequencies, as is shown in Fig. 2. This can be intuitively understood in terms of the geometrical picture of a WGM: a WGM is a mode confined in a microdisk by total internal reflections occurring at the dielectric/air interface and that, additionally, satisfies the round trip condition.
The resonance frequencies of the modes with p = 1 are then:

$$2\pi R = m\frac{\lambda}{n} = m\frac{2\pi c}{n\omega} \tag{7}$$

High p modes have their "center of mass" displaced towards the microdisk center, so that, for these modes, we can always use equation (7) but with a smaller "effective radius" R. As equation (7) suggests, once m is fixed, this results in a higher mode frequency.
If the resonance frequencies are known, expression (4) allows to obtain the radial function $\psi(\rho)$ for TM or TE modes. At this point, we can write the independent field component E_x or H_x, since the functions $\Theta(\theta)$ and G(x) are already known.
Once E_x or H_x is found, the other field components can be directly obtained by using Maxwell's equations:

TM modes

$$\begin{cases} H_\rho = \dfrac{m}{\mu_0 \rho \tilde{\omega}} E_x \\ H_\theta = -\dfrac{j}{\mu_0 \tilde{\omega}} \dfrac{\partial E_x}{\partial \rho} \end{cases} \tag{8}$$

TE modes

$$\begin{cases} E_\rho = -\dfrac{m}{\varepsilon_0 \varepsilon \rho \tilde{\omega}} H_x \\ E_\theta = \dfrac{j}{\varepsilon_0 \varepsilon \tilde{\omega}} \dfrac{\partial H_x}{\partial \rho} \end{cases} \quad (9)$$

If the vertical part fulfills the condition

$$\int_{-\infty}^{+\infty} G^2(x)dx = 1 \quad (10)$$

then the constant N in equation (4) can be chosen in order to normalize the mode to the azimuthal power flow:

TM modes

TE modes

$$P_\theta = \begin{cases} +\dfrac{1}{2}\mathrm{Re}\left(\int_0^\infty E_x H_\rho^* d\rho\right) \\ -\dfrac{1}{2}\mathrm{Re}\left(\int_0^\infty E_\rho H_x^* d\rho\right) \end{cases} \quad (11)$$

2.2 Quality factor

The Q-factor of a resonance physically represents the number of optical cycles needed before its original energy decays by 1/e in the absence of further sourcing; this means that if U is the energy stored in the cavity, then we have:

$$\frac{dU}{dt} = -\frac{\omega}{Q} U \quad (12)$$

Since the term –dU/dt represents the dissipated power P_d, we find an alternative definition of Q:

$$Q = \omega \frac{U}{P_d} \quad (13)$$

On the other hand, Q can be written in the following form (Srinivasan, 2006):

$$Q = \omega \tau_{ph} = \frac{2\pi n_g L_{ph}}{\lambda} \quad (14)$$

where τ_{ph} is the photon lifetime, L_{ph} is the cavity decay length and n_g is the group index within the cavity.

Equation (14) is a useful relation because it allows to compare the losses of a microcylinder with those of other devices (e.g. a planar waveguide): in fact, for a planar waveguide it is customary to write the losses in terms of an inverse decay length α (in cm^{-1}). Once we know the resonance quality factor, we can use this equation to obtain L_{ph} and then express the losses in the form $\alpha = 1/L_{ph}$.

Until now, the only loss mechanism introduced for the microcylinder resonances was represented by the intrinsic radiation losses responsible for the finite value of Q_{WGM}. In

physical experiments, the situation is slightly more complex, and additional losses affect the overall Q-factor of a WGM.
Under the hypothesis that all loss factors are so small that their effects on the intra-cavity field can be treated independently, the overall quality factor can be written in the following form:

$$\frac{1}{Q}=\frac{1}{Q^{WGM}}+\frac{1}{Q^{mat}}+\frac{1}{Q^{cpl}}=\frac{1}{Q^{int}}+\frac{1}{Q^{cpl}} \tag{15}$$

Q^{cpl} represents the losses due to an eventual external coupling (see section 3), and Q^{mat} quantifies the losses due to bulk absorption. In the linear regime, this can be the case of free-carrier absorption, whereas, in the nonlinear regime, this term could include two-photon (or, in general, multi-photon) absorption. In the latter case, Q^{mat} will then depend on the field intensity circulating inside the cavity.
Both Q^{WGM} and Q^{mat} are intrinsic terms, whereas the last part of equation (15) describes the external coupling. In the next section, we will use the coupled mode theory for a thorough study of the evanescent coupling of a microcylinder and a bus waveguide or fiber; for the moment, the discussion is limited to a qualitative picture. Looking at Fig. 3, we can imagine to inject a given power into the fundamental mode of a single-mode waveguide sidecoupled to the microcylinder. In the region where the two structures almost meet, the exponential tail of the waveguide mode overlaps the WGM giving rise to an evanescent coupling.

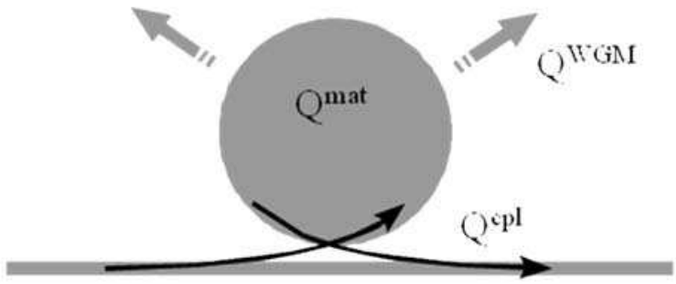

Fig. 3. Evanescent coupling scheme with a bus waveguide.

A final remark concerns the fact that the intrinsic quality factor Q^{int} can be reduced by additional contributions, e.g. the surface loss terms caused by surface scattering and surface absorption (Borselli et al., 2005). For this reason, we will denote with Q^{rad} (and not Q^{WGM}) the radiation losses.
Surface losses cannot always be neglected and become dominant in particular situations; moreover, they give rise to important phenomena like the lift of degeneracy for standingwave WGMs.

3. Three-wave mixing in semiconductor microcylinders

Microcavities are very promising for nonlinear optics applications, thanks to the high optical quality factors attainable with today's technology. For example, the group of J. D. Joannopoulos at MIT proved that high quality photonic crystal resonators can be very effective in obtaining low-power optical bistable switching (Soljačić et al., 2002), Second-Harmonic Generation (SHG), and in modifying the bulk nonlinear susceptibility through the Purcell effect (Soljačić et al., 2004; Bravo-Abad et al., 2007).

For nonlinear optics applications, the advantage of having a high-Q resonator is that its modes are stored in the cavity for many optical periods: this provides a considerable interaction time between modes and can be used to enhance parametric interactions.
WGM resonators are particularly well suited to attain high Q: for example, quality factors as high as $Q = 5 \times 10^6$ and $Q = 3.6 \times 10^5$ have been reported, at telecom wavelengths, for Si (Borselli et al., 2005) and AlGaAs (Srinivasan et al., 2005) microdisks, respectively.
In a DFG process, two pumps of frequencies ω_1 and ω_2 interact in order to generate a signal at the frequency difference $\omega_3 = \omega_1 - \omega_2$: in this way, energy conservation is ensured at photon level.
In this context, the exploitation of GaAs offers peculiar advantages with respect to other materials. Apart from having a wide transparency range, large refractive index, and a huge nonlinear coefficient, GaAs has in fact highly mature growth and fabrication technologies, and offers attracting possibilities in terms of optoelectronic integration and electrical pumping. On the other hand, due to its optical isotropy, GaAs-based nonlinear applications normally require technologically demanding phase-matching schemes (Levi et al., 2002). These are not necessary in the case of WGM resonators since, as theoretically demonstrated for a second harmonic generation process (Dumeige & Feron, 2006; Yang et al., 2007), the symmetry of a [100]-grown AlGaAs microdisk and the circular geometry of the cavity result in a periodic modulation of the effective nonlinear coefficient experienced by the interacting WGMs. This modulation can then be used to phase-match the pump and the generated fields without additional requirements.
The evanescent coupling between a semiconductor microcylinder and a waveguide is a way to excite two pump WGMs inside the microcavity. This technique has already been adopted in our laboratory for the characterization of GaAs microdisks.
In Fig. 4 we report the top view of a cylindrical cavity of radius R side-coupled to a bus waveguide used to inject two pump fields at ω_1 and ω_2. The intracavity generated field could be extracted by using a second waveguide, and the waveguide/microcavity distances can be chosen to optimize the injection/extraction efficiency.
The difference frequency generation in a triply resonant microcylinder can be described using the standard coupled mode theory.
The set of coupled mode theory equations describing this nonlinear process is (Haus, 1984):

$$\begin{cases} \dfrac{da_1}{dt} = j\omega_1 a_1 - \dfrac{a_1}{\tau_1^{tot}} + j\sqrt{\dfrac{2}{\tau_1^{tot}}}s_1 - s_1^{NL} \\ \dfrac{da_2}{dt} = j\omega_2 a_2 - \dfrac{a_2}{\tau_2^{tot}} + j\sqrt{\dfrac{2}{\tau_2^{tot}}}s_2 - s_2^{NL} \\ \dfrac{da_3}{dt} = j\omega_3 a_3 - \dfrac{a_3}{\tau_3^{tot}} - s_3^{NL} \end{cases} \quad (16)$$

For the i-th resonant mode (i = 1, 2, 3), a_i is the mode amplitude normalized to its energy, $\tau_i^{tot} = 2Q_i^{tot}/\omega_i$ is the total photon lifetime (including intrinsic and coupling losses). The terms s_i describe the external pumping, with $|s_i|^2 = P_i^{in}$ (P_i^{in} being the input power in the bus waveguide).
The third equation is slightly different since the WGM field at ω_3, which is generated inside the cavity, is not injected from the outside: its source is then constituted by the nonlinear

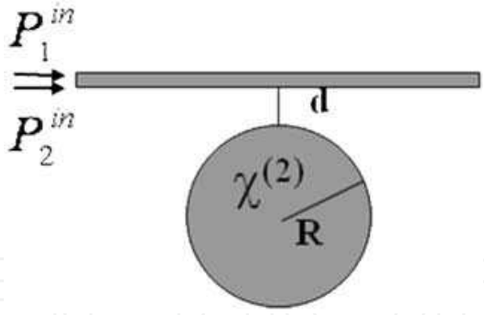

Fig. 4. Top view of a microcylinder coupled to an input waveguide.

term s_3^{NL}. For typical values like the ones we will see in the following, the pump depletion can be ignored, i.e. we can neglect the terms s_i^{NL} with i = 1,2.

In this way, putting $a_i = A_i e^{j\omega_i t}$ and looking for the steady state solution of the two pumps, we find:

$$|A_i|^2 = \frac{4}{\omega_i} \frac{Q_i^{cpl}}{\left(1 + Q_i^{cpl}/Q_i^{int}\right)^2} P_i^{in} \tag{17}$$

Where Q_i^{cpl} is the loss term due to the presence of the coupling to the waveguide, and Q_i^{int} the intrinsic quality factor, with $1/Q^{tot} = 1/Q^{int} + 1/Q^{cpl}$.

Equation (17) suggests that the power transfer from the waveguide to the cavity can be adjusted by changing the coupling losses, i.e. by properly varying the distance between waveguide and microcylinder and/or reducing the width of the waveguide. This transfer is maximized under critical coupling ($Q_i^{cpl} = Q_i^{int}$).

The power fed into the mode at ω_3 is:

$$P_3 = -\frac{j\omega_3}{4} \int \vec{E}^*(\omega_3) \cdot \vec{P}^{NL}(\omega_3) dV + c.c. \tag{18}$$

where c.c. denotes the complex conjugate, and $\vec{P}^{NL}$ is the nonlinear polarization given by:

$$P_i^{NL}(\omega_3) = \varepsilon_0 \sum_{jk} \chi_{ijk}^{(2)} E_j(\omega_1) E_k^*(\omega_2) \tag{19}$$

By using equations (18) and (19) we can rewrite s_3^{NL} in the form:

$$s_3^{NL} = -\frac{j\omega_3}{4} a_1 a_2^* I_{ov} \tag{20}$$

where I_{ov} is the nonlinear overlap integral between the WGMs:

$$I_{ov} = \varepsilon_0 \int_V \sum_{ijk} \chi_{ijk}^{(2)} E_i^*(\omega_3) E_j(\omega_1) E_k^*(\omega_2) dV \tag{21}$$

with V the cavity volume and $\chi^{(2)}$ the nonlinear tensor.

The $\bar{4}3m$ GaAs symmetry (Palik, 1999) and the growth axis in the [100] direction imply that the overlap integral differs from zero only when two of the three WGMs are TE polarized

and one is TM polarized. Moreover, the angular part of the integral in equation (20) can be readily calculated, resulting in the phase-matching condition $\Delta m = m_2 + m_3 - m_1 \pm 2 = 0$.
The $\pm$ 2 is due to the additional momentum provided by the periodic modulation of the $\chi^{(2)}$ coefficient that comes from the circular geometry of the cavity.
Looking for the steady state solution of the field at ω_3, and taking into account equation (17), we then find:

$$\left|A_3\right|^2 = \frac{(\omega_3/4)^2}{\left(1/\tau_3^{tot}\right)^2}\prod_{i=1}^{2}\left[\frac{4}{\omega_i}\frac{Q_i^{cpl}}{\left(1+Q_i^{cpl}/Q_i^{int}\right)^2}\right]\left|I_{ov}\right|^2 P_1^{in}P_2^{in} \tag{22}$$

Therefore, if the difference-frequency mode is extracted with an additional waveguide, and under the hypothesis that the critical coupling condition is fulfilled for the three WGMs, the generated power is:

$$P_3^{cpl} = \frac{2\left|A_3\right|^2}{\tau_3^{cpl}} = \frac{1}{16}\frac{\omega_3}{\omega_1\omega_2}Q_1^{int}Q_2^{int}Q_3^{int}\left|I_{ov}\right|^2 P_1^{in}P_2^{in} \tag{23}$$

On the other hand, if the intracavity-generated field is not coupled to any waveguide (it is simply radiated) and under the hypothesis of critical coupling for the two pumps, we find:

$$P_3^{rad} = \frac{2\left|A_3\right|^2}{\tau_3^{rad}} = \frac{1}{4}\frac{\omega_3}{\omega_1\omega_2}\frac{1}{Q_3^{rad}\left(1/Q_3^{rad}+1/Q_3^{mat}\right)^2}Q_1^{int}Q_2^{int}\left|I_{ov}\right|^2 P_1^{in}P_2^{in} \tag{24}$$

We see that, in both cases, the non linear efficiency is directly related to the overlap between the three interacting fields and it is enhanced proportionally to the time the mode spend inside the resonator: higher Q-factors result in a longer interaction time between the fields in the nonlinear mixing.

4. Nonlinear GaAs Microcylinder for Terahertz Generation

4.1 Introduction

In the field of Terahertz spectroscopy there is a clear distinction between the broad-band time-domain spectroscopy (TDS) and the single-frequency (CW) spectroscopy. In TDS, the THz source is often a photoconductive dipole antenna excited by femtosecond lasers: by Fourier transforming the incident and transmitted optical pulses, it is possible to obtain the dispersion and absorption properties of the sample under investigation. This technique has proven powerful to study the far-infrared properties of various components, like dielectrics and semiconductors (Grischkowsky et al., 1990) or gases (Harde & Grischkowsky, 1991), and for imaging (Hu & Nuss, 1995).
However, besides requiring costly and often voluminous mode-locked lasers, the principal drawback of the THz TDS relies on its limited frequency resolution ($\Delta\nu \sim 5$ GHz) resulting from the limited time window ($\Delta t \sim 100$ ps), (Sakai, 2005).
On the other hand, narrow-band THz systems have found many applications in atmospheric and astronomical spectroscopy, where a high spectral resolution (1−100 MHz) is generally required (Siegel, 2002).
Among the large number of proposed CW-THz source schemes, it is worth mentioning at least two. The first one, known as photo-mixing, makes use of semi-insulating or

lowtemperature grown GaAs (Sakai, 2005). However, no significant progress in terms of output power has been demonstrated in CW photoconductive generation during the last few years, and the maximum output powers are in the 100 nW range.
The second CW scheme is the Quantum Cascade Laser (QCL) (Faist et al., 1994): in this case, the photons are emitted by electron relaxations between quantum well sub-bands. The original operating wavelength was $\lambda = 4.2$ μm and was extended in the THz region (Kohler et al., 2002). However, the main drawback of this kind of sources is that they are poorly tunable and only operate at cryogenic temperatures.
An alternative and interesting approach for the generation and amplification of new frequencies, both pulsed and CW, is based on second-order nonlinear processes: in this case, the first THz generation from ultrashort near-infrared pulses was demonstrated in bulk nonlinear crystals such as ZnSe and $LiNbO_3$ (Yajima & Takeuchi, 1970).
In 2006 Vodopyanov et al. demonstrated the generation of 0.9 to 3 THz radiation in periodically inverted GaAs, with optical to THz conversion efficiencies of 10^{-3} (Vodopyanov, 2006). With respect to terahertz generation in $LiNbO_3$ (Kawase et al., 2002), GaAs constitutes a privileged material choice, thanks to its large nonlinearity and inherently low losses at THz frequencies (~ 1 cm^{-1}). However, the periodically inversed GaAs sources are neither compact nor easy to use outside research laboratories, since they require bulky mode-locked pump sources. To avoid this technological complexity, it has been proposed to exploit the anomalous dispersion created by the phonon absorption band in GaAs to phase match a difference-frequency generation in the terahertz range (Berger & Sirtori, 2004).
In 2008 Vodopyanov and Avetisyan reported generation of terahertz radiation in a planar waveguide: using an optical parametric oscillator operating near 2 μm (with average powers of 250 and 750 mW for pump and idler), the THz output was centered near 2 THz and had 1 μW of average power (Vodopyanov & Avetisyan, 2008).
In the same year, Marandi et al. proposed a novel source of continuous-wave terahertz radiation based on difference frequency generation in GaAs crystal. This source is an integration of a dielectric slab and a metallic slit waveguide. They predicted an output power of 10.4 μW at 2 THz when the input infrared pumps have a power of 500 mW (Marandi et al., 2008).
In this section, we will present a CW, room-temperature THz source based on DFG from two near-IR WGMs in a high-quality-factor GaAs microcylinder: these pump modes are excited by the emission of quantum dots (QDs) embedded in the resonator.
The cavity, as sketched in Fig. 5, is a cylinder composed of a central GaAs layer sandwiched between two lower-index AlAs layers, capped on both sides by a metallic film (e.g. Au). This configuration provides both vertical dielectric confinement for the near-IR pump modes and plasmonic confinement for the THz mode. The design stems from two opposite

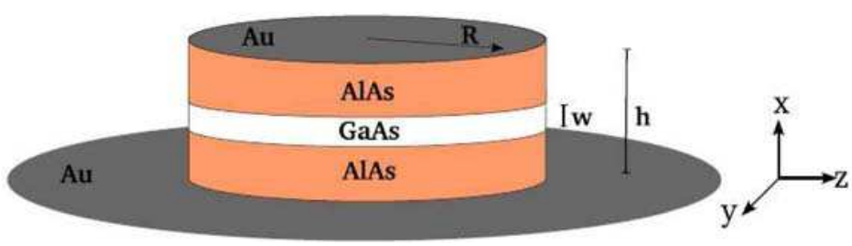

Fig. 5. Sketch of a GaAs/AlAs microcylinder.

requirements on the thickness of AlAs layers, aimed at increasing the DFG efficiency: maximize the overlap between the interacting modes, and prevent the exponential tails of the near-IR modes from reaching the metallic layers, thus avoiding detrimental absorption losses.
Fig. 6 shows an example of the pump and THz mode profile.

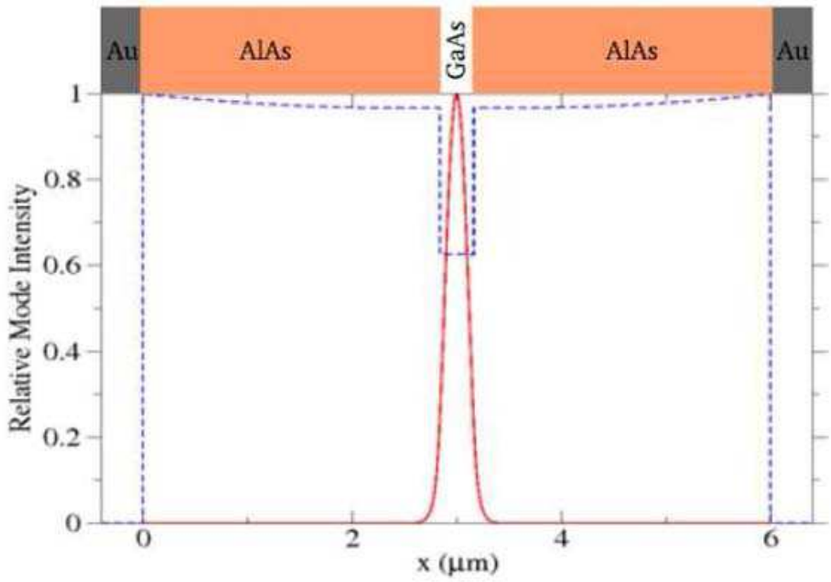

Fig. 6. Example of the vertical near-IR (solid line) and THz (dashed line) mode profiles. The wavelength are λ = 0.9 μm e λ = 70.0 μm for the IR e THz mode respectively.

The double metal cap allows to strongly confine the THz mode: with respect to a structure with just a top metallic mirror, where the THz mode would leak into the substrate, this allows to increase the overlap between the WGMs, thus improving the conversion efficiency.
In the horizontal plane, the light is guided by the bent dielectric/air interface, which gives rise to high-Q WGMs (Nowicki-Bringuier et al., 2007). The central GaAs layer contains one or more layers of self-assembled InAs quantum dots, which excite the two near-IR modes, and can be pumped either optically or electrically. The simultaneous lasing of these modes, without mode competition, can be obtained thanks to the inhomogeneously broadened gain curve of the QD ensemble, as observed for QDs in microdisks at temperatures as high as 300K (Srinivasan, 2005), and in microcylinders (Nowicki-Bringuier et al., 2007).
Fig. 7 shows the micro-photoluminescence (μPL) spectra of a 4 μm diameter pillar containing QDs reported in (Nowicki-Bringuier et al., 2007). The number next to each peak corresponds to the azimuthal number of a TE WGM excited by the QD ensemble emission. The figure also shows that increasing the pillar diameter results in a reduced free spectral range: if the structure diameter is big enough, it is possible to find two WGM whose frequency difference lies in the THz range.
In order to find the WGM spectrum of the cavity shown in Fig. 5, we can use the effective index method described in the previous sections: as demonstrated in (Nowicki-Bringuier et al., 2007), this approach gives an excellent approximation for micropillar WGMs.

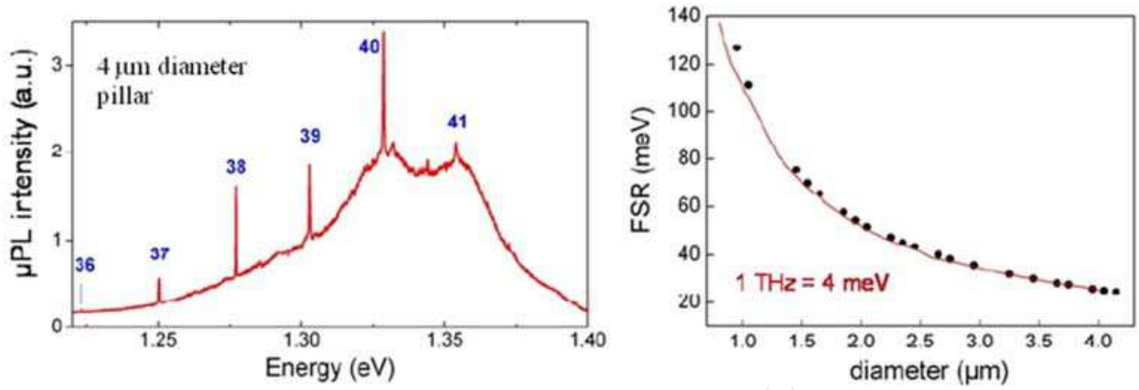

Fig. 7. Left: experimental μPL spectra measured at 4K on a 4 μm diameter pillar. Right: calculated (solid line) and observed (filled points) free spectral range versus diameter (Nowicki-Bringuier et al., 2007).

Applying the coupled mode theory to the present case, we obtain the following equation for the THz mode amplitude a_3:

$$\frac{da_3}{dt} = j\omega_3 a_3 - \left(\frac{1}{\tau_3^{rad}} + \frac{1}{\tau_3^{mat}}\right) a_3 + s_3^{NL} \tag{25}$$

where τ_3^{rad} (τ_3^{mat}) represents the radiation (material absorption) limited photon lifetime. Again, the s_3^{NL} term represents the nonlinear polarization source, and it is given by (20). As mentioned before, in order to generate the third mode, we have to fulfill two conditions:

1. two of the three WGMs must be TE polarized and one TM polarized;
2. the phasematching condition $\Delta m = m_2 + m_3 - m_1 \pm 2 = 0$ must hold.

If A_3 is the steady state solution of (25), the radiated THz power is:

$$P_3^{rad} = \frac{2|A_3|^2}{\tau_3^{rad}} = \frac{\omega_3}{4} \frac{Q_3^{rad}}{\left(1 + Q_3^{rad}/Q_3^{mat}\right)^2} U_1 U_2 |I_{ov}|^2 \tag{26}$$

with U_1 and U_2 the electromagnetic energy stored in the two pump WGMs and I_{ov} the nonlinear overlap integral given by (21).
This shows that the emitted THz power is proportional to the energy of the pump modes, and it can be increased by maximizing the overlap integral between the interacting WGMs.
As a final remark, we stress that the quality factor of the THz mode is mainly limited by intrinsic (radiation and material) losses. Conversely, intrinsic losses are extremely small for near-IR WGMs; therefore these modes will display experimentally quality factors that are limited by extrinsic losses, such as scattering by sidewall roughness (Srinivasan et al., 2005; Nowicki-Bringuier et al., 2007).

4.2 Numerical results

By numerically studying (Andronico et al., 2008) the structure of Fig. 5 with w = 0.325 μm and h = 6 μm, we find that a radius R = 40.6 μm allows to phase-match two pumps near 1 μm (λ_1 = 0.923 μm and λ_2 = 0.936 μm) and a THz WGM with λ_3 = 63.385 μm (i.e. ν_3 = 4.8 THz). The corresponding azimuthal numbers are m_1 = 917, m_2 = 913 and m_3 = 2. For the two

pump modes, we took AlGaAs dispersion into account according to the Gehrsitzs model (Gehrsitzs et al., 2000).
Since the dipole of the fundamental transition in the InAs QDs is oriented in the microcylinder plane (Cortez et al., 2001), the only WGMs excited by the QDs are TE polarized. The THz WGM has then to be a TM mode.
Moreover, unlike quantum wells, the gain curve of QD ensembles is mostly broadened due to QD size fluctuations (inhomogeneous broadening). For InAs QDs in GaAs, the latter is 60-100 meV, and is centered around 1.3 eV (λ = 0.95 μm), (Nowicki-Bringuier et al., 2007). Such inhomogeneous broadening is thus much larger than the homogeneous broadening (10 meV at room-temperature (Cortez et al., 2001)): this allows to have different WGMs simultaneously lasing, with no mode competition (Siegman, 1986).
Under the hypothesis of Q = 10^5 for the two pump modes for AlGaAs microdisks with embedded QDs, we can make important statements for our source: 1) its estimated phasematching width, dictated by the finesse of the near-IR WGMs, is 3 GHz; 2) under the conservative assumption of extracting 1 mW (corresponding to a circulating power of 16 W) from each of the pump modes, the emitted THz power, calculated from equation (25), is expected to be about 1 μW.
It is also interesting to observe that, at these pump powers, two-photon absorption does not affect the performance of our device and can be safely neglected in the calculations.
Fig. 8 shows the far-field pattern of the source at room temperature obtained with a semianalytic method developed following (Heebner et al., 2007). The emission is concentrated at high angles, due to the strong diffraction experienced by the tightly confined THz mode.

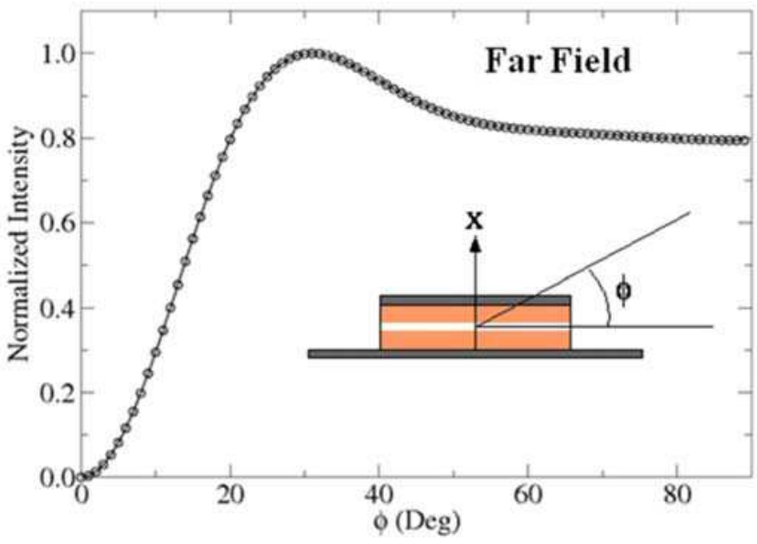

Fig. 8. Far Field pattern of the THz microcylinder source at room temperature, emitting at λ_3 = 63.4 μm. The inset shows the coordinate system used.

In Fig. 9 we report the effect of radius fabrication tolerance on the generated THz frequency, for three different temperatures: the slight THz frequency shift resulting from non-nominal fabrication is comparable to the phase-matching spectral width, and it is therefore negligible. Once the temperature has been chosen, each point in Fig. 14 corresponds to a

phase-matched triplet with fixed azimuthal and radial numbers on each curve (different for each temperature).

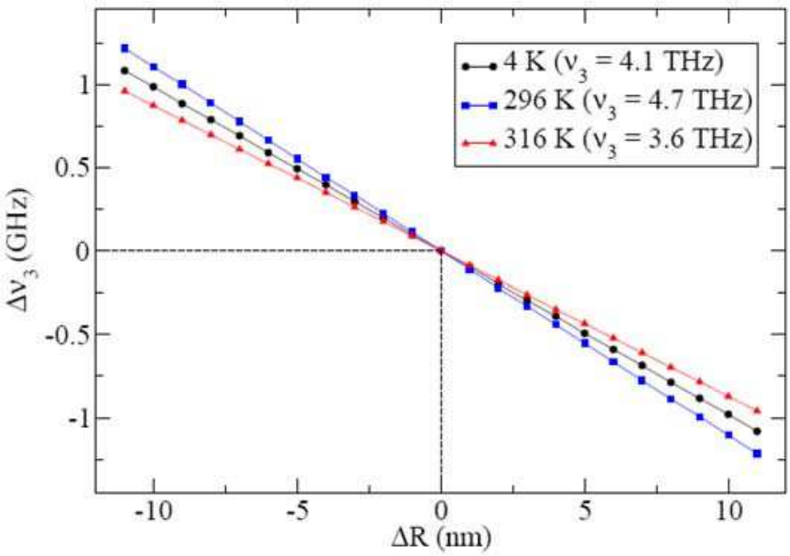

Fig. 9. Frequency deviation from nominal case ν_3 versus radius tolerance, for three different temperatures: 4K (circles), 296K (squares) and 316K (triangles).

A final remark concerns the wavelength range covered by this device: there are in fact two independent factors that contribute to it. As previously stated, at 300K, the homogeneous broadening of QDs is of the order of 10meV (Borri et al., 2001), which restricts the THz generation to frequencies $\nu_3 > 2.4$ THz. Emission at lower frequencies can be obtained by reducing the QDs homogeneous broadening, at the expense of a low-temperature operation. Conversely, the upper limit is set by the GaAs Rest-Strahlen band, i.e. $\nu_3 < 6$ THz.
In conclusion, this THz source is based on intracavity three-wave mixing between WGMs. As compared to the other THz sources today available, it could have noteworthy characteristics, such as: 1) room-temperature operation; 2) relatively high output power; 3) compactness; and 4) fabrication simplicity.

5. Perspectives

Being based on a cylindrical geometry, our THz source results in a compact and solid device, which provides a natural and elegant solution to combine the vertical confinement of the near-IR WGMs and THz mode. The two mirrors optimize the spatial overlap between the THz and the near-infrared modes, thus providing efficient conversion.
The presence of the QDs as active medium also allows, as an interesting perspective, to electrically pump the two near-IR modes. This can be accomplished by modifying the structure as shown in Fig. 10: the p-doped top and the n-doped bottom AlGaAs slabs allow the current flow. Besides their use as mirrors, the metallic layers are then exploited as external electrical contacts of the structure. Moreover, in order to selectively inject the current in the outer part of the cylinder where the near-infrared WGMs are located, a highly resistive region is defined by ion implantation in the central part of the cavity.

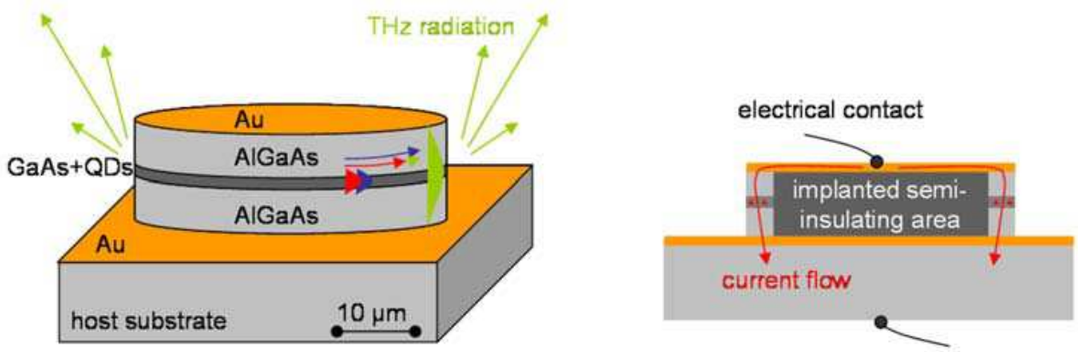

Fig. 10. Side view and cross section of microcylinder for electrical injection.

Compared to the standard air-suspended microdisk, the microcylinder geometry comes with a few crucial advantages, and it is well suited to achieve the high power lasing necessary to increase the efficiency of the nonlinear conversion process. Indeed, the heat sinking is significantly better than in air-suspended microdisks, where heating degrades the lasing properties (mode shifts, power saturation).

Moreover, although electrical pumping of microdisk lasers has been reported (Fujita et al. 2000), the lasing performances are strongly limited by the fact that the current is injected through the disk pedestal near the center of the microdisk. In the microcylinder geometry, the current can be selectively injected at the circumference of the GaAs active layer, which sustains the WGM modes.

Up to now, the lasing of WGMs in micropillars has been demonstrated only at low temperature and under optical pumping. Structures enabling THz confinement and a selective electrical injection at the edges of the microcylinder still need some technological progress, in order to minimize the threshold current, and optimize the lasing properties of the WGM modes under high injection conditions.

Although Q-factors in the 10^4 range have already been observed in similar structures (Nowicki-Bringuier et al., 2007), further improvement would ameliorate the lasing properties of the microcylinder, and increase the intensity of the near-IR light that is stored in the cavity.

To conclude, it is worth stressing that our source offers other interesting possibilities, as more long term developments: (a) the use of other semiconductors like the widely exploited InGaAsP/InP system; (b) a microcylinder with a single top mirror: to vertically confine the THz in the microcylinder a doped layer could be used below the AlAs layer, replacing the bottom mirror. This configuration is technologically simpler to realize; however, the THz mode would inevitably leak into the substrate, and we also expect a reduced efficiency due to a reduced overlap integral; (c) the incorporation of a quantum cascade structure: quantum cascade devices can simultaneously laser on two frequencies, without mode competition (Franz et al., 2007). This dual emission could then provide the two pumps needed in the DFG. Nevertheless, since the intersubband selection rules only allow TM polarized light, we could not use the [100] direction as growth axis, but we could replace it with the [111] direction (Berger & Sirtori, 2004); (d) a multi-spectral emission with lithographically defined arrays of microcylinders; (e) the fabrication of phased-array architectures by adjusting the distance between the microcylinders: this would allow to control the far-field pattern of the device; (f) optical pumping the device by approaching a fiber.

6. References

Andronico, A.; Claudon, J.; Gerard, J. M.; Berger, V. & Leo, G. (2008). Integrated Terahertz Source based on Three-Wave Mixing of Whispering-Gallery Modes. *Optics letters*, Vol. 33, No. 21, (October 2008) pp. 2416-2418, ISSN 0146-9592

Armaroli, A.; Morand, A.; Benech, P.; Bellanca, G. & Trillo, S. (2008). Three-Dimensional Analysis of Cylindrical Microresonators Based on the Aperiodic Fourier Modal Method. *Journal Optical Society America A*, Vol. 15, No. 8, (March 2008) pp. 667-675, ISSN 1084-7529

Berger, V. & Sirtori, C. (2004). Nonlinear Phase Matching in THz Semiconductor Waveguides. *Semiconductor Science and Technology*, Vol. 19, No. 8, (June 2004) pp. 964-970, ISSN 0268-1242

Borri, P.; Langbein, W.; Schneider, S.; Woggon, U.; Sellin, R. L.; Ouyang, D. & Bimberg, D. (2001). Ultralong Dephasing Time in InGaAs Quantum Dots. *Physical Review Letters*, Vol. 87, No. 15, (October 2001) pp. 157401.1–157401.4, ISSN 0031-9007

Borselli, M.; Johnson, T. J. & Painter, O. (2005). Beyond the Rayleigh Scattering Limit in High-Q Silicon Microdisk: Theory and Experiment. *Optics Express*, Vol. 13, No. 5, (March 2005) pp. 1515-1530, ISSN 1094-4087

Boyd, R. W. (2003). *Nonlinear Optics*, Academic Press, ISBN 0-12-121682-9, New York

Bravo-Abad, J.; Rodriguez, A.; Bermel, P.; Johnson, S. J.; Joannopoulos, J. D. & Soljačić, M. (2007). Enhanced Nonlinear Optics in Photonic-Crystal Microcavities. *Optics Express*, Vol. 15, No. 24, (November 2007) pp. 16161-16176, ISSN 1094-4087

Cortez, S.; Krebs, O.; Voisin, P. & Gerard, J. M. (2001). Polarization of the Interband Optical Dipole in InAs/GaAs Self-Organized Quantum Dots. *Physical Review B*, Vol. 63, No. 23, (May 2001) pp. 233306.1–233306.4, ISSN 0163-1829

Dumeige, Y. & Feron, P. (2006). Whispering-Gallery-Mode Analysis of Phase-Matched Doubly Resonant Second-Harmonic Generation. *Physical Review A*, Vol. 74, No. 6, (December 2006) pp. 063804.1-063804.7 ,ISSN 1050-2947

Faist, J.; Capasso, F.; Sivco, D. L.; Sirtori, C.; Hutchinson, A. L. & Cho, A. Y. (1994). Quantum Cascade Laser. *Science*, Vol. 264, No. 5158, (April 1994) pp. 553 556, ISSN 1095-9203

Franz, K. J. ; Wasserman, D. ; Hoffman, A. J.; Jangraw, D. C. ; Shiu, K.-T.; Forrest, S. R. & Gmachl, C. (2007). Evidence of Cascaded Emission in a Dual-Wavelength Quantum Cascade Laser. *Applied Physics Letters*, Vol. 90, No. 9, (February 2007) pp. 091104.1–091104.3, ISSN 0003-6951

Fujita, M.; Ushigome, R. & Baba, T. (2000). Continuous Wave Lasing in GaInAsP Microdisk Injection Laser with Threshold Current of 40 μA. *Electronics Letters*, Vol. 36, No. 9, (April 2000) pp. 790–791, ISSN 0013-5194

Gehrsitz S.; Reinhart, F. K.; Gourgon, C.; Herres, N.; Vonlanthen, A. & Sigg, H. (2000). The Refractive Index of $Al_xGa_{1-x}As$ below the Band Gap: Accurate Determination and Empirical Modeling. *Journal of Applied Physics*, Vol. 87, No. 11, (June 2000) pp. 7825-7837, ISSN 0021-8979

Grischkowsky, D.; Keiding, S.; Van Exter, M. & Fattinger, C. (1990). Far-Infrared Time-Domain Spectroscopy with Terahertz Beams of Dielectrics and Semiconductors. *Journal of Optical Society of America B*, Vol. 7, No. 10, (October 1990) pp. 2006–2015, ISSN 0740-3224

Haus, H. A. (1984). *Waves and Fields in Optoelectronics*. Prentice-Hall, ISBN 0-13-946053-5, New Jersey

Harde, H. & Grischkowsky, D. (1991). Coherent Transients Excited by Subpicosecond Pulses of Terahertz Radiation. *Journal of the Optical Society of America B*, Vol. 8, No. 8, (August 1991) pp. 1642-1651, ISSN 0740-3224

Heebner, J. E.; Bond, T. C. & Kallman, J. S. (2007). Generalized Formulation for Performance Degradations due to Bending and Edge Scattering Loss in Microdisk Resonators. *Optics Express*, Vol. 15, No. 8, (April 2007) pp. 4452-4473, ISSN 1094-4087

Hu, B. B. & Nuss, M. C. (1995). Imaging with THz Waves. *Optics Letters*, Vol. 20, No. 16, (August 1995) pp. 1716-1718, ISSN 0146-9592

Kawase, K.; Minamide, H.; Imai, K.; Shikata, J. & Ito, J. (2002). Injection- Seeded Terahertz-Wave Parametric Generator with Wide Tunability. *Applied Physics Letters*, Vol. 80, No. 2, (January 2002) pp. 195–197, ISSN 0003-6951

Kohler, R.; Tredicucci, A; Beltram, F.; Beere, H.; Linfield, E. H.; Davies, A. G.; Ritchie, D. A.; Iotti, R. C. & Rossi, F. (2002). Terahertz Semiconductor-Heterostructure Laser. *Nature*, Vol. 417, No. 6885, (May 2002) pp. 156-159, ISSN 0028-0836

Levi, O.; Pinguet, T. J.; Skauli, T.; Eyres, L. A.; Parameswaran, K. R.; Harris, J. S. J.; Fryer, M. M.; Kulp, T. J.; Bisson, S. E.; Gerard, B.; Lallier E. & Becouarn L. (2002). Difference Frequency Generation of 8 1m Radiation in Orientation-Patterned GaAs. *Optics Letters*, Vol. 32, No. 7, (December 2002) pp. 2091-2093, ISSN 0146-9592

Marandi, A.; Darcie, T. E. & So, P. P. M. (2008). Design of a Continuous-Wave Tunable Terahertz Source using Waveguide-Phase-Matched GaAs. *Optics Express*, Vol. 16, No. 14, (July 2008) pp. 10427-10433, ISSN 1094-4087

Mittleman, D. (2003). *Sensing with Terahertz Radiation*, Springer-Verlag, ISBN 3-540-43110-1, Berlin

Nowicki-Bringuier, Y.-R.; Claudon, J.; Bockler, C.; Reitzenstein, S.; Kamp, M.; Morand, A.; Forchel, A. & Gerard, J. M. (2007). High Q Whispering Gallery Modes in GaAs/AlAs Pillar Microcavities. *Optics Express*, Vol. 15, No. 25, (December 2007) 17291–17304, ISSN 1094-4087

Palik, E. D. (1998). *Handbook of optical constants of solids*, Academic Press, ISBN 0-12-544423-0, New York

Sakai, K. (2005). *Terahertz optoelectronics*, Springer-Verlag, ISBN 3-540-20013-4, Berlin

Siegel, P. H. (2002). Terahertz Technology. *IEEE Microwave Theory and Techniques Society*, Vol. 50, No. 3, (March 2002) pp.910–928, ISSN 0018–9480

Siegman, A. E. (1986). *Lasers*, University Science Books, ISBN 0-935702-11-3, Mill Valley

Soljačić, M.; Ibanescu, M.; Johnson, S. G.; Fink, Y. & Joannopoulos J. D. (2002). Optimal Bistable Switching in Nonlinear Photonic Crystals. *Physical Review E*, Vol. 66, No. 5, (November 2002) pp. 055601.1-0.55601.4, ISSN 1539-3755

Soljačić, M. & Joannopoulos, J. D. (2004). Enhancement of Nonlinear Effects Using Photonic Crystal. *Nature Materials*, Vol. 3, No. 4, (April 2004) pp. 211-219, ISSN 1476-1122

Srinivasan, K.; Borselli, M.; Johnson, T. J.; Barclay, P. E.; Painter, O; Stintz, A. & Krishna, S. (2005). Optical Loss and Lasing Characteristics of High-Quality-Factor AlGaAs Microdisk Resonators with Embedded Quantum Dots. *Applied Physics Letters*, Vol. 86, (April 2005) 151106: 1-3, ISSN 0003-6951

Srinivasan, K. (2006). Semiconductor Optical Microcavities for Chip-Based Cavity QED, Ph.D. thesis, California Institute of Technology.

Tamir, T. (1990). *Guided-Wave Optoelectronics*, Springer-Verlag, ISBN 3-540-52780-x, Berlin

Tonouchi, M. (2007). Cutting-edge terahertz technology. *Nature Photonics*, Vol. 1, No. 2, (February 2007) pp. 97-105, ISSN 1749-4893

Vodopyanov, K. L.; Feyer, M. M., Yu, X.; Harris, J. S.; Lee, Y.-S.; Hurlbut, W. C.; Kozlov, V. G.; Bliss, D. & Lynch, C. (2006). Terahertz-Wave Generation in Quasi Phase-Matched GaAs. *Applied Physics Letters*, Vol. 89, No. 14, (October 2006) pp. 141119.1-141119.3, ISSN 0003-6951

Vodopyanov, K. L. & Avetisyan, Yu. H. (2008). Optical Terahertz Wave Generation in a Planar GaAs Waveguide. *Optics Letters*, Vol. 33, No. 20, (October 2008), pp. 2314-2316, ISSN 0146-9592

Yajima, T. & Takeuchi, N. (1970). Far-Infrared Difference-Frequency Generation by Picosecond Laser Pulses. *Japanese Journal of Applied Physics*, Vol. 9, No. 11, (June 1970) pp. 1361–1371, ISSN 0021-4922

Yang, Z.; Chak, P.; Bristow, A. D.; Van Driel, H. M.; Iyer, R.; Aitchison, J. S.; Smirl, A. L.; Sipe, J. E. (2007). Enhanced Second-Harmonic Generation in AlGaAs Microring Resonators. *Optics Letters*, Vol. 32, No. 7, (April 2007) pp. 826-828, ISSN 0146-9592

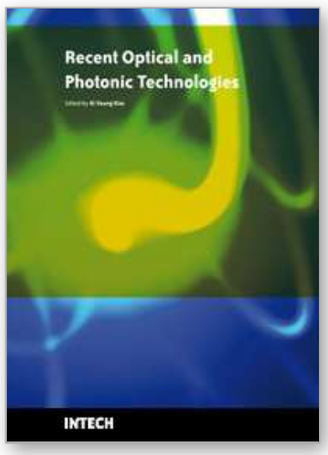

Recent Optical and Photonic Technologies

Edited by Ki Young Kim

ISBN 978-953-7619-71-8
Hard cover, 450 pages
Publisher InTech
Published online 01, January, 2010
Published in print edition January, 2010

Research and development in modern optical and photonic technologies have witnessed quite fast growing advancements in various fundamental and application areas due to availability of novel fabrication and measurement techniques, advanced numerical simulation tools and methods, as well as due to the increasing practical demands. The recent advancements have also been accompanied by the appearance of various interdisciplinary topics. The book attempts to put together state-of-the-art research and development in optical and photonic technologies. It consists of 21 chapters that focus on interesting four topics of photonic crystals (first 5 chapters), THz techniques and applications (next 7 chapters), nanoscale optical techniques and applications (next 5 chapters), and optical trapping and manipulation (last 4 chapters), in which a fundamental theory, numerical simulation techniques, measurement techniques and methods, and various application examples are considered. This book deals with recent and advanced research results and comprehensive reviews on optical and photonic technologies covering the aforementioned topics. I believe that the advanced techniques and research described here may also be applicable to other contemporary research areas in optical and photonic technologies. Thus, I hope the readers will be inspired to start or to improve further their own research and technologies and to expand potential applications. I would like to express my sincere gratitude to all the authors for their outstanding contributions to this book.

InTech Europe
University Campus STeP Ri
Slavka Krautzeka 83/A
51000 Rijeka, Croatia
Phone: +385 (51) 770 447

InTech China
Unit 405, Office Block, Hotel Equatorial Shanghai
No.65, Yan An Road (West), Shanghai, 200040, China
中国上海市延安西路65号上海国际贵都大饭店办公楼405单元
Phone: +86-21-62489820

Fax: +385 (51) 686 166
www.intechopen.com

Fax: +86-21-62489821

IntechOpen